CMS Physics Analysis Summary

Contact: cms-pag-conveners-heavyions@cern.ch 2014/05/20

Long-range two-particle correlations with K^0_S and $\Lambda/\overline{\Lambda}$ in pPb and PbPb collisions

The CMS Collaboration

Abstract

Measurements of two-particle angular correlations between identified strange hadrons (K^0_S and $\Lambda/\overline{\Lambda}$) and unidentified charged particles, emitted in pPb collisions, are presented over a wide range in pseudorapidity and full azimuth. The data, corresponding to an integrated luminosity of approximately $35 nb^{-1}$, were collected during the 2013 LHC pPb run at a nucleon-nucleon center-of-mass energy of 5.02TeV by the CMS experiment. The results are compared to 2.76TeV semi-peripheral PbPb collision data, collected during the 2011 PbPb run, covering a similar range of particle multiplicities. The K^0_S and $\Lambda/\overline{\Lambda}$ are reconstructed via their topological secondary decays. The observed long-range correlations are characterized by the second-order (v_2) and third-order (v_3) anisotropy harmonics of K^0_S and $\Lambda/\overline{\Lambda}$, which are studied as a function of particle multiplicity and transverse momentum. For high-multiplicity pPb events, a particle-species dependence of v_2 and v_3 is observed. Divided by the number of constituent quarks, the v_2 and v_3 harmonics of K^0_S and $\Lambda/\overline{\Lambda}$ as a function of kinetic energy per quark fall on the same curve within 10–15% for each multiplicity class. This scaling is better than that observed in peripheral PbPb collisions.

1 Introduction

Studies of multiparticle correlations provide important insights to the underlying mechanism of particle production in high-energy collisions of protons and nuclei. In relativistic nucleus-nucleus (AA) collisions, the observed long-range, two-particle correlations, characterized by a pronounced structure at $|\Delta\phi| \approx 0$ that extends over a large $\Delta\eta$ range, have been extensively explored at both the Relativistic Heavy Ion Collider (RHIC) [1–5] and the Large Hadron Collider (LHC) [6–10], over a wide range of energies and system sizes. Here, $\Delta\phi$ and $\Delta\eta$ are the differences in azimuthal angle ϕ and pseudorapidity $\eta = -\ln[\tan(\theta/2)]$ between the two particles, where the polar angle θ is determined relative to the clockwise circulating beam. Long-range correlations in AA collisions are believed to mainly arise from the collective flow of a strongly interacting, expanding medium [11]. In hydrodynamic models, the detailed azimuthal correlation structure of emitted particles is typically characterized by its Fourier components, $\sim 1 + 2\sum_n v_n^2 \cos(n\Delta\phi)$, where v_n denote the single-particle anisotropy harmonics [12]. In particular, the second and third Fourier components, known as elliptic (v_2) and triangular (v_3) flow, respectively, most directly reflect the medium response to the initial collision geometry and to its fluctuations [13], providing insight into fundamental transport properties of the medium [14–16].

Similar long-range correlations have been recently discovered in proton-proton (pp) [17] and proton-lead (pPb) [18–20] collisions with very high final-state particle multiplicity at the LHC. Evidence of such correlations is also found in 200 GeV deuteron-gold (dAu) collisions at RHIC [21]. While it is widely accepted that this long-range structure in large AA systems is a consequence of collective flow, its origin in small collision systems is still unclear. A variety of theoretical models have been proposed to interpret this phenomenon in pp (see Ref. [22] for a recent review) and pPb collisions. Besides hydrodynamic effects in the high-density system possibly formed in these collisions at TeV energies [23, 24], the theory of gluon saturation in the initial interaction of the protons has also been shown to describe the long-range correlation data [25, 26]. To better differentiate among the various theoretical scenarios, measurements have been made of the elliptic and triangular flow harmonics of unidentified charged particles from long-range correlations, and compared to hydrodynamic calculations for pPb collisions [27, 28].

Elliptic flow of identified particles measured in AA collisions at RHIC exhibits an intriguing dependence on the particle species [29, 30]. For transverse momentum (p_{T}) below about 2 GeV, the v_2 of heavier particles (e.g., protons) is observed to be smaller than that of lighter particles (pions) [31, 32]. This mass ordering effect of v_2 in AA collisions is expected in hydrodynamic models [33–35] due to stronger radial flow of heavier particles. Evidence of such mass ordering is recently found also in pPb collisions [36], which can also be described by hydrodynamics in pPb [37, 38]. Moreover, in AA collisions at RHIC, a remarkable number of constituent quark scaling phenomenon is discovered for v_2 over low and intermediate p_{T} ranges (up to $p_{\mathrm{T}} \approx 5$–6 GeV) [39, 40], where the v_2 Fourier harmonic as a function of the transverse kinetic energy ($KE_{\mathrm{T}} = m_T - m$, where $m_T = \sqrt{m^2 + p_{\mathrm{T}}^2}$), scales with the number of constituent quarks n_q in a hadron. That is, when v_2/n_q is plotted as a function of KE_{T}/n_q for each type of meson ($n_q = 2$) and baryon ($n_q = 3$), the curves approximately coincide. This simple scaling law may indicate that the elliptic flow is developed first among quarks before they recombine into hadrons [41–43], providing evidence of deconfinement of quarks and gluons in high-energy AA collisions. It is of high interest to look for such quark number scaling of azimuthal correlations in smaller collision systems like pp and pPb.

To provide new insights on understanding the particle production mechanism in high-multiplicity

pPb collision system, this paper presents a detailed analysis of two-particle correlations with identified strange hadrons of K^0_S and $\Lambda/\overline{\Lambda}$ in pPb collision at $\sqrt{s_{NN}}$ = 5.02 TeV. With the implementation of a dedicated high-multiplicity trigger, the 2013 pPb data sample gives access to a multiplicity comparable to that in mid-central PbPb collisions (e.g., $\sim$ 55% centrality, where centrality is defined as the fraction of the total inelastic cross section, with 0% denoting the most central collisions). The anisotropy harmonics v_2 and v_3 are extracted from long-range two-particle correlations by associating a K^0_S or $\Lambda/\overline{\Lambda}$ particle with another unidentified charged particle, as a function of particle p_T and event multiplicity. The ratios of v_2 and v_3 to the number of constituent quarks are obtained as a function of hadron transverse kinetic energy per quark for both K^0_S and $\Lambda/\overline{\Lambda}$, to examine the validity of constituent quark number scaling that is originally observed in AA collisions at RHIC. Furthermore, a direct comparison of pPb and PbPb data over a broad range of similar multiplicities is presented.

2 CMS experiment and data sample

A description of the Compact Muon Solenoid (CMS) detector can be found in Ref. [44]. The main detector component used in this paper is the inner tracker, located in a superconducting solenoid of 6 m internal diameter, providing a magnetic field of 3.8 T. The inner tracker consists of 1440 silicon pixel and 15 148 silicon strip detector modules. It measures charged particles within the pseudorapidity range $|\eta| < 2.5$, and provides an impact parameter resolution of $\sim$15 μm and a transverse momentum (p_T) resolution of about 1.5% for 100 GeV particles.

Also located inside the solenoid are the electromagnetic calorimeter (ECAL) and hadron calorimeter (HCAL). The ECAL consists of 75 848 lead-tungstate crystals, arranged in a quasi-projective geometry and distributed in a barrel region ($|\eta| < 1.48$) and two endcaps that extend to $|\eta| = 3.0$. The HCAL barrel and endcaps are sampling calorimeters composed of brass and scintillator plates, covering $|\eta| < 3.0$. Iron/quartz-fiber Cerenkov hadron forward (HF) calorimeters cover the range $2.9 < |\eta| < 5.2$ on either side of the interaction region. The detailed Monte Carlo (MC) simulation of the CMS detector response is based on GEANT4 [45].

The data sample used in this analysis is collected by CMS during the LHC pPb run in 2013. The total integrated luminosity of the data set is about 35 nb^{-1}, based on the pPb interaction cross section determined in Ref. [46]. The beam energies are 4 TeV for protons and 1.58 TeV per nucleon for lead nuclei, resulting in a center-of-mass energy per nucleon pair of 5.02 TeV. The direction of the higher energy proton beam is initially set up to be clockwise, and is then reversed. As a result of the energy difference between the colliding beams, the nucleon-nucleon center-of-mass in the pPb collisions is not at rest with respect to the laboratory frame. Massless particles emitted at $\eta_{cm} = 0$ in the nucleon-nucleon center-of-mass frame will be detected at $\eta = -0.465$ (clockwise proton beam) or 0.465 (counterclockwise proton beam) in the laboratory frame. A sample of peripheral 2.76 TeV PbPb data collected during the 2011 LHC heavy-ion run, corresponding to an integrated luminosity of 2.3 μb^{-1}, is also analyzed for comparison with pPb data at similar multiplicity ranges.

3 Online triggering and offline reconstruction and selection

The online triggering and the offline reconstruction and selection follow the same procedure as is established in Ref. [28], where more details can be found.

Minimum bias (MB) pPb events are triggered by requiring at least one track with $p_T > 0.4$ GeV to be found in the pixel tracker for a pPb bunch crossing. Because of hardware limits on the

data acquisition rate, only a small fraction ($\sim 10^{-3}$) of all minimum bias triggered events are recorded. In order to collect a large sample of high-multiplicity pPb collisions, a dedicated high-multiplicity trigger is implemented using the CMS level-1 (L1) and high-level trigger (HLT) systems. At L1, the total transverse energy summed over ECAL and HCAL is required to be greater than a given threshold (20 or 40 GeV). Charged tracks are then reconstructed online at the HLT based on the three layers of pixel detectors, by requiring a track origin within a cylindrical region of length 30 cm along the beam and radius 0.2 cm perpendicular to the beam. For each event, the vertex reconstructed with the highest number of pixel tracks ($N_{\mathrm{trk}}^{\mathrm{online}}$) is selected. The $N_{\mathrm{trk}}^{\mathrm{online}}$ is determined by pixel tracks with $|\eta| < 2.4$, $p_{\mathrm{T}} > 0.4\,\mathrm{GeV}$, and a distance of closest approach of 0.4 cm or less to this vertex, and is required to exceed a certain threshold for an event to be recorded. Data are taken with thresholds of $N_{\mathrm{trk}}^{\mathrm{online}} > 100, 130$ (L1 threshold of 20 GeV), and 160, 190 (L1 threshold of 40 GeV) with prescaling factors dependent on the instantaneous luminosity. The $N_{\mathrm{trk}}^{\mathrm{online}} > 190$ trigger is never prescaled throughout the entire run.

In the offline analysis, hadronic collisions are selected by requiring a coincidence of at least one HF calorimeter tower with more than 3 GeV of total energy in both HF detectors. Events are also required to contain at least one reconstructed primary vertex within 15 cm of the nominal interaction point along the beam axis and within 0.15 cm transverse to the beam trajectory. At least two reconstructed tracks are required to be associated with the primary vertex. Beam related background is suppressed by rejecting events for which less than 25% of all reconstructed tracks are of good quality (i.e., of the quality of the tracks selected for physics analysis as will be discussed later). The pPb instantaneous luminosity provided by the LHC in the 2013 run resulted in approximately 3% probability of having at least one additional interaction present in the same bunch crossing (pileup events). A procedure for rejecting pileup events is described in Ref. [28] based on the number of tracks associated with each reconstructed vertex and the distance between different vertices. A purity of 99.8% for single pPb collision event is achieved for the highest multiplicity pPb interactions studied in this paper. With the selection criteria above, 97–98% of the events are found to be selected among those pPb interactions simulated with the EPOS [47] and HIJING [48] event generators that have at least one primary particle with total energy $E > 3\,\mathrm{GeV}$ in both η ranges of $-5 < \eta < -3$ and $3 < \eta < 5$.

In this analysis, the CMS *highPurity* [49] tracks are used to select primary-track candidates. Additional requirements are also applied to enhance the purity of primary tracks. The significance of the separation along the beam axis (z) between the track and the best vertex, $d_z/\sigma(d_z)$, and the significance of the impact parameter relative to the best vertex transverse to the beam, $d_{\mathrm{T}}/\sigma(d_{\mathrm{T}})$, must be less than 3, and the relative uncertainty of the transverse-momentum measurement, $\sigma(p_{\mathrm{T}})/p_{\mathrm{T}}$, must be less than 10%. Additionally, the CMS *loose* [49] tracks are also used to incorporate secondary-track candidates with larger track impact parameters, for reconstructing $\mathrm{K}^0_{\mathrm{S}}$ and $\Lambda/\overline{\Lambda}$ candidates (as will be described in Sec. 4). To ensure high tracking efficiency and to reduce the rate of misidentified tracks, only tracks with $|\eta| < 2.4$ and $p_{\mathrm{T}} > 0.3\,\mathrm{GeV}$ are used in the analysis (a different p_{T} cutoff of 0.4 GeV is used in the multiplicity determination because of constraints on the online processing time for the high-level trigger). Based on simulation studies using GEANT4, the combined geometrical acceptance and efficiency for primary track reconstruction exceeds 60% for $p_{\mathrm{T}} \approx 0.3\,\mathrm{GeV}$ and $|\eta| < 2.4$. The efficiency is greater than 90% in the $|\eta| < 1$ region for $p_{\mathrm{T}} > 0.6\,\mathrm{GeV}$. For the event multiplicity range studied in this paper, no dependence of the tracking efficiency on multiplicity is found and the rate of misreconstructed tracks remains at the 1–2% level.

The entire pPb data set is divided into classes of reconstructed track multiplicity, $N_{\mathrm{trk}}^{\mathrm{offline}}$, where primary tracks with $|\eta| < 2.4$ and $p_{\mathrm{T}} > 0.4\,\mathrm{GeV}$ are counted. Details of the multiplicity classifi-

cation in this analysis, including the fractional cross section and the average number of primary tracks before and after correcting for detector effects in each multiplicity range, are provided in Ref. [28]. A subset of peripheral PbPb data collected during the 2011 LHC heavy-ion run with a minimum bias trigger are also reanalyzed in order to directly compare pPb and PbPb systems at the same collision multiplicity. This PbPb sample is reprocessed using the same event selections and track reconstruction algorithm as for the present pPb analysis although a different trigger is used. A description of the 2011 PbPb data can be found in Ref. [28, 50].

4 Reconstruction of K^0_S and $\Lambda/\overline{\Lambda}$ candidates

The reconstruction technique of K^0_S and $\Lambda/\overline{\Lambda}$ candidates (generally referred to as V^0s) at CMS was first developed in Ref. [51]. Oppositely charged tracks with transverse and longitudinal impact parameter significances greater than 1 are first selected to form a good vertex. The distance at the closest approach of the pair of tracks is required to be less than 0.5 cm. The fitted vertex of each pair of tracks is required to have a χ^2 value normalized by the degree of freedom less than 7. The pair of two tracks are assumed to be $\pi^+\pi^-$ in K^0_S reconstruction, while the assumption of $\pi^- p(\pi^+\bar{p})$ is used in Λ ($\overline{\Lambda}$) reconstruction. For $\Lambda/\overline{\Lambda}$, the lower momentum track is assumed to be the pion.

Due to the long lifetime of K^0_S and $\Lambda/\overline{\Lambda}$ particles, a cut on the significance of V^0 decay length, which is the three-dimensional distance between primary and V^0 vertex, to be greater than 5 is applied to further suppress the background. To remove K^0_S misidentified as $\Lambda/\overline{\Lambda}$ and vice versa, the $\Lambda/\overline{\Lambda}$ (K^0_S) candidates must have a corresponding $\pi^+\pi^-(p\pi^-)$ mass more than 20 (10) MeV away from the world-average K^0_S ($\Lambda/\overline{\Lambda}$) mass. To reduce $\Lambda/\overline{\Lambda}$ contribution from weak decay of Ξ and Ω^-, the V^0 momentum vector is required to point back to the primary vertex. This is achieved by imposing a cut of $\cos\theta^{\text{point}} > 0.999$, where θ^{point} is the angle between the V^0 momentum vector and the vector connecting primary and V^0 vertices. Residual $\Lambda/\overline{\Lambda}$ from weak decays after applying this cut is estimated to be less than 3% from MC simulations. The K^0_S and $\Lambda/\overline{\Lambda}$ reconstruction efficiency is about 6% and 1% at $p_T \approx 1$ GeV, and reaches about 20% and 10% above p_T =3–4 GeV, respectively. The relatively low reconstruction efficiency of the V^0 candidates is primarily due to the tight cuts applied in suppressing the background candidates, and also the low efficiency of reconstructing daughter tracks below $p_T \approx 0.3$ GeV.

An example of invariant mass distributions of reconstructed K^0_S and $\Lambda/\overline{\Lambda}$ candidates are shown in Fig. 1 for 5.02 TeV pPb data, with V^0 p_T range of 1–3 GeV in multiplicity range $220 \leq N^{\text{offline}}_{\text{trk}} < 260$. The V^0 peaks can be clearly identified with little background. The true V^0 signal peak is well described by a double Gaussian function (with a common mean), while the background is modeled by a 4th-order polynomial function. The mass window of $\pm 2\sigma$ wide around the center of the peak is defined as the "peak region", where σ represents the standard deviation of the double Gaussian function (with typical value of σ indicated in Fig. 1). To estimate the contribution of background candidates in the peak region to the correlation measurement, a "sideband region" is also chosen including V^0 candidates outside $\pm 3\sigma$ mass range around the peak up to the limit of the mass distributions shown in Fig. 1.

5 Analysis technique of two-particle correlations

The construction of two-particle correlation function follows the same procedure established in Refs. [6, 7, 18, 28]. However, in this paper, reconstructed V^0 candidates from either the peak or sideband region are taken as "trigger" particles within a given p_T^{trig} range, instead of charged

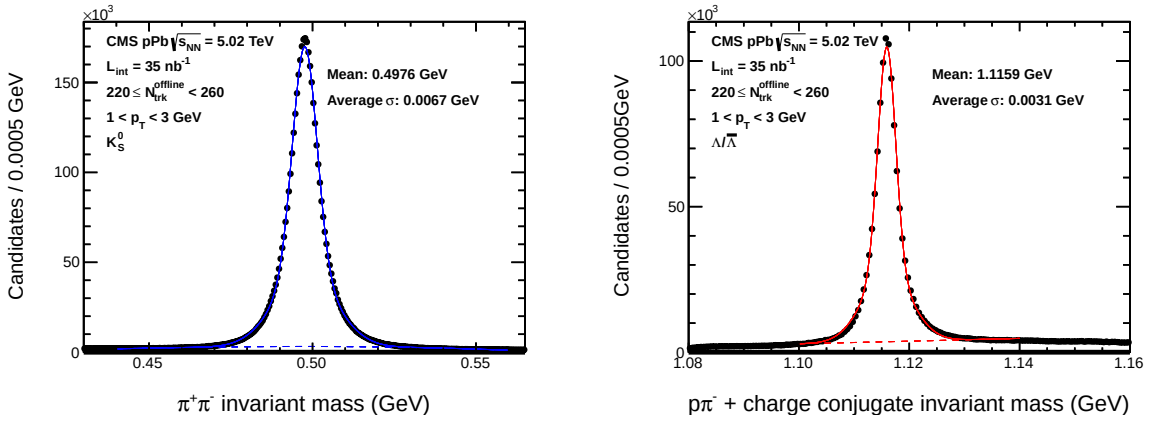

Figure 1: Invariant mass distribution of K^0_S (left) and $\Lambda/\overline{\Lambda}$ (right) candidates in the p_T range of 1–3 GeV for $220 \leq N^{\text{offline}}_{\text{trk}} < 260$ in pPb collisions at $\sqrt{s_{NN}} = 5.02$ TeV. The solid line shows the fit function of a double Gaussian plus a 4th-order polynomial. The number of candidates in the peak region for this p_T and multiplicity range is about 3.32 million for K^0_S and 0.95 million for $\Lambda/\overline{\Lambda}$.

tracks as used in previous publications. The number of trigger V^0 candidates in the event is denoted by N_{trig}. Particle pairs are then formed by associating each trigger particle with the remaining charged primary tracks from a specified p_T^{assoc} interval (which can be either the same as or different than the p_T^{trig} range). The two-dimensional (2D) per-trigger-particle associated yield is defined in the same way as previous analyses

$$\frac{1}{N_{\text{trig}}}\frac{d^2N^{\text{pair}}}{d\Delta\eta d\Delta\phi} = B(0,0) \times \frac{S(\Delta\eta,\Delta\phi)}{B(\Delta\eta,\Delta\phi)}, \tag{1}$$

where $\Delta\eta$ and $\Delta\phi$ are the differences in η and ϕ of the pair. The same-event pair distribution, $S(\Delta\eta,\Delta\phi)$, represents the yield of particle pairs normalized by N_{trig} from the same event,

$$S(\Delta\eta,\Delta\phi) = \frac{1}{N_{\text{trig}}}\frac{d^2N^{\text{same}}}{d\Delta\eta d\Delta\phi}\,. \tag{2}$$

The mixed-event pair distribution,

$$B(\Delta\eta,\Delta\phi) = \frac{1}{N_{\text{trig}}}\frac{d^2N^{\text{mix}}}{d\Delta\eta d\Delta\phi}\,, \tag{3}$$

is constructed by pairing the trigger V^0 candidates in each event with the associated charged particles from 20 different randomly selected events in the same 2 cm wide z_{vtx} range and from the same track multiplicity class. Here, N^{mix} denotes the number of pairs taken from the mixed events. The ratio $B(0,0)/B(\Delta\eta,\Delta\phi)$ mainly accounts for pair-acceptance effects, with $B(0,0)$ representing the mixed-event associated yield for both particles of the pair going in approximately the same direction and thus having full pair acceptance (with a bin width of 0.3 in $\Delta\eta$ and $\pi/16$ in $\Delta\phi$). A pair is removed if the associated particle belongs to a daughter track of any trigger V^0 candidate (this contribution is negligible since associated particles are mostly primary tracks, while V^0 daughter tracks are mostly secondary).

The same-event and mixed-event pair distributions are first calculated for each event, and then averaged over all the events within the track multiplicity class. The range of $0 < |\Delta\eta| < 4.8$

and $0 < |\Delta\phi| < \pi$ is used to fill one quadrant of the $(\Delta\eta, \Delta\phi)$ histograms, with the other three quadrants filled (for illustration purposes) by reflection to cover a $(\Delta\eta, \Delta\phi)$ range of $-4.8 < \Delta\eta < 4.8$ and $-\pi/2 < \Delta\phi < 3\pi/2$ for the 2D correlation functions, as will be shown later in Fig. 2. In performing the correlation analyses, each reconstructed primary track and V^0 candidate is weighted by a correction factor, respectively, following the procedure described in Refs. [6, 7, 18, 28]. This factor accounts for detector effects including the reconstruction efficiency, the detector acceptance, and the fraction of misreconstructed tracks. However, this correction is found to have a negligible effect on the azimuthal anisotropy harmonics.

5.1 Extraction of v_n harmonics

Motivated by hydrodynamic models of long-range correlations in pPb collisions, azimuthal anisotropy harmonics of K^0_S and $\Lambda/\overline{\Lambda}$ particles are extracted via a Fourier decomposition of $\Delta\phi$ correlation functions averaged over $|\Delta\eta| > 2$,

$$\frac{1}{N_{\text{trig}}}\frac{\mathrm{d}N^{\text{pair}}}{\mathrm{d}\Delta\phi} = \frac{N_{\text{assoc}}}{2\pi}\left[1 + \sum_n 2V_{n\Delta}\cos(n\Delta\phi)\right], \tag{4}$$

as is done in Refs. [6, 7, 18, 28], where $V_{n\Delta}$ are the Fourier coefficients and N_{assoc} represents the total number of pairs per trigger V^0 particle for a given $(p_{\text{T}}^{\text{trig}}, p_{\text{T}}^{\text{assoc}})$ bin. The first three Fourier terms are included in the fits to the correlation functions. Including additional terms has a negligible effect on the results of the Fourier fit. A minimum $|\Delta\eta|$ of 2 units is applied to remove short-range correlations from jet fragmentation.

If the observed two-particle azimuthal correlations in pPb collisions are mainly originated from hydrodynamic flow effects, the $V_{n\Delta}$ coefficients can be factorized into the product of single-particle anisotropy v_n for trigger and associated particles, respectively,

$$V_{n\Delta}(p_{\text{T}}^{\text{trig}}, p_{\text{T}}^{\text{assoc}}) = v_n(p_{\text{T}}^{\text{trig}}) \times v_n(p_{\text{T}}^{\text{assoc}}). \tag{5}$$

Following this assumption, the elliptic and triangular anisotropy harmonics, v_2 and v_3, of V^0 particles can be extracted as a function of p_{T} from the fitted Fourier coefficients,

$$v_n(p_{\text{T}}^{V^0}) = \frac{V_{n\Delta}(p_{\text{T}}^{V^0}, p_{\text{T}}^{\text{ref}})}{\sqrt{V_{n\Delta}(p_{\text{T}}^{\text{ref}}, p_{\text{T}}^{\text{ref}})}}, \qquad n = 2, 3. \tag{6}$$

Here, a fixed $p_{\text{T}}^{\text{ref}}$ range for the "reference" charged primary particles is chosen to be $0.3 < p_{\text{T}} < 3.0\,\text{GeV}$ to minimize correlations from jets at higher p_{T}.

The v_n values are first extracted for V^0 candidates from the peak region (which contains contribution of background V^0s) and sideband region, denoted as v_n^{obs} and v_n^{bkg}, respectively. The final goal of this paper is to obtain the v_n signal of true V^0 particles, denoted as v_n^{sig}. It can be then calculated as

$$v_n^{\text{sig}} = \frac{v_n^{\text{obs}} - (1 - f^{\text{sig}}) \times v_n^{\text{bkg}}}{f^{\text{sig}}}, \qquad n = 2, 3, \tag{7}$$

assuming v_n^{sig} and v_n^{bkg} are independent from each other. Here, f^{sig} represents the signal yield fraction in the peak region determined by the fits to the mass distribution shown in Fig. 1. This fraction exceeds 80% for $\Lambda/\overline{\Lambda}$ at $p_{\mathrm{T}} > 1\,\mathrm{GeV}$ and is above 95% for $\mathrm{K}^0_{\mathrm{S}}$ over the entire p_{T} range.

5.2 Systematic uncertainties

The dominant sources of systematic uncertainties are related to the reconstruction of V^0 candidates. No evident p_{T} dependence of systematic effects on the results is found so the estimated systematic uncertainties are assumed to be constant percentages over the entire p_{T} range. The fit range to the V^0 mass distributions (Fig. 1) is varied, which yields a systematic uncertainty of less than 1% to the v_2^{sig} result. By varying the invariant mass range of the peak region from $\pm 1\sigma$ to $\pm 3\sigma$, the v_2^{sig} value is found to be consistent within 2%. Systematic uncertainties due to selection of different sideband mass regions is estimated to be 2.2%. Possible contamination of residual mis-identified V^0 candidates (i.e., $\mathrm{K}^0_{\mathrm{S}}$ as $\Lambda/\overline{\Lambda}$, and vice versa) is also investigated. By varying the invariant mass range for rejecting the mis-identified V^0 candidates, the v_2^{sig} result is consistent within 2%. Systematic uncertainties related to selections of the V^0 candidates are evaluated by tightening or loosening the cuts on the decay length significance and $\cos\theta^{\mathrm{point}}$, which shows an agreement better than 3%. As misalignment of the tracker geometry can affect the V^0 reconstruction performance, an alternative misalignment configuration was studied and found to have less than a 2% effect on v_2^{sig}.

To test the procedure of extracting V^0 signal v_2 from Eq. 7, study using EPOS pPb MC events is performed to compare the v_2^{sig} results with generator-level $\mathrm{K}^0_{\mathrm{S}}$ and $\Lambda/\overline{\Lambda}$ v_2 derived by the two-particle correlation technique. The agreement is found to be better than 4%. Other systematic uncertainties introduced by high-multiplicity trigger efficiency (1%) and possible residual pileup effect (1–2%) for pPb data are estimated in the same way as in Ref. [28], and found to have a small contribution. Various sources of systematic uncertainties are added together in quadrature to arrive at final systematic uncertainties (6.9% for pPb and 6.6% for PbPb), which are shown as boxes in the figures. Systematic uncertainties of v_3^{sig} data are quoted to be the same as those of v_2^{sig}, as is done in Ref. [28].

6 Results

The 2D two-particle correlation functions measured in 5.02 TeV pPb collisions for pairs of a $\mathrm{K}^0_{\mathrm{S}}$ (left) or $\Lambda/\overline{\Lambda}$ (right) trigger particle from the peak region and a charged associated particle ($h^{\pm}$) are shown in Fig. 2 in the p_{T} range of 1–3 GeV. Here, the 2D correlation functions are also corrected for the background V^0 candidates, following the same approach of correcting v_n in Eq. 7. However, this correction is negligible in this p_{T} range because of the high signal yield fraction of V^0 candidates. For low-multiplicity events ($N_{\mathrm{trk}}^{\mathrm{offline}} < 35$, Fig. 2 (a) and (b)), a sharp peak near $(\Delta\eta, \Delta\phi) = (0, 0)$ due to jet fragmentation (truncated for better illustration of the full correlation structure) can be clearly observed for both $\mathrm{K}^0_{\mathrm{S}}$–$h^{\pm}$ and $\Lambda/\overline{\Lambda}$–$h^{\pm}$ correlations. Moving onto high-multiplicity events ($220 \leq N_{\mathrm{trk}}^{\mathrm{offline}} < 260$, Fig. 2 (c) and (d)), besides the peak from jet fragmentations, a pronounced long-range structure is seen at $\Delta\phi \approx 0$ extending at least 4.8 units in $|\Delta\eta|$. This structure was previously observed in high-multiplicity ($N_{\mathrm{trk}}^{\mathrm{offline}} \sim 110$) pp collisions at $\sqrt{s} = 7$ TeV [17] and pPb collisions at $\sqrt{s_{NN}} = 5.02$ TeV [18–20, 28] for unidentified charged particles, and also for identified charged pions, kaons and protons in pPb collisions at $\sqrt{s_{NN}} = 5.02$ TeV [36]. This long-range correlation structure has also been extensively studied in AA collisions over a wide range of energies [1–9], and is believed to arise primarily from collective flow of a strongly interacting medium [12].

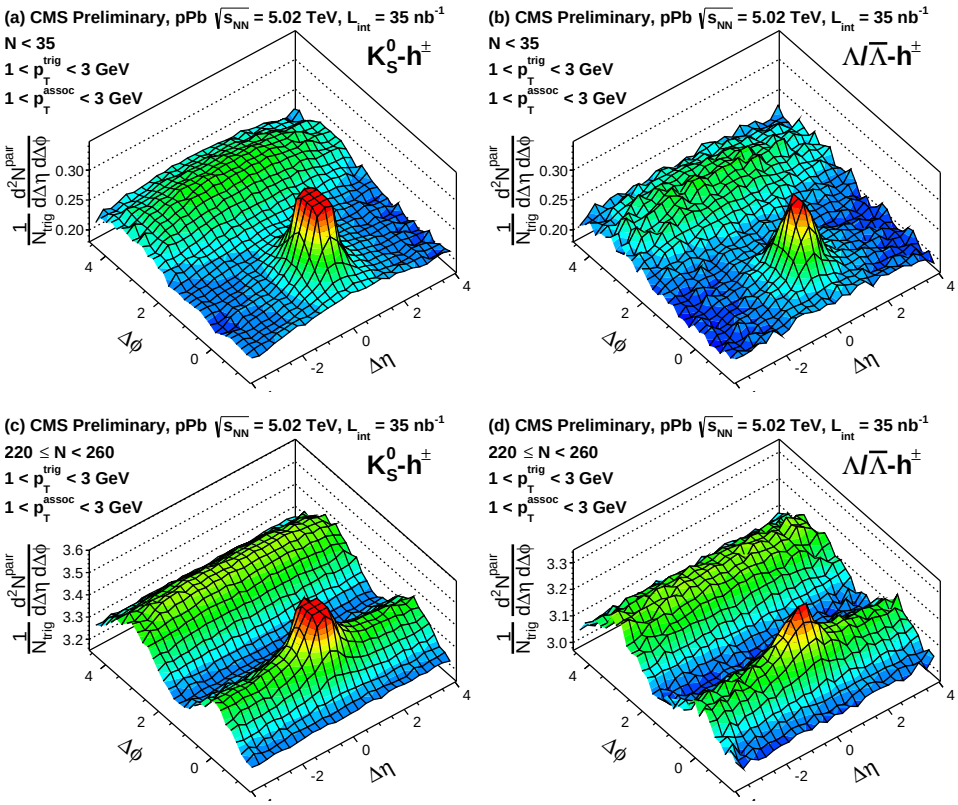

Figure 2: The 2D two-particle correlation functions for 5.02 TeV pPb collisions for pairs of a K^0_S (a,c) or $\Lambda/\overline{\Lambda}$ (b,d) trigger particle and a charged associated particle ($h^{\pm}$), with $1 < p_T^{trig} < 3\,GeV$ and $1 < p_T^{assoc} < 3\,GeV$, in the multiplicity ranges $N_{trk}^{offline} < 35$ (a, b) and $220 \leq N_{trk}^{offline} < 260$ (c, d). The sharp near-side peak from jet correlations is truncated to emphasize the structure outside that region.

To investigate the correlation structure for different species of particles in quantitative detail, one-dimensional (1D) distributions in $\Delta\phi$ are found by averaging the signal and mixed-event 2D distributions over $|\Delta\eta| < 1$ (defined as the "short-range region") and $|\Delta\eta| > 2$ (defined as the "long-range region"), as done in Refs. [6, 7, 17, 18, 28]. Figure 3 shows the 1D $\Delta\phi$ correlation functions of pPb data for unidentified charged particle (left), K^0_S (middle) and $\Lambda/\overline{\Lambda}$ (right) as a trigger, in the multiplicity range $N_{trk}^{offline} < 35$ (open) and $220 \leq N_{trk}^{offline} < 260$ (filled). The curves show the Fourier fits from Eq. (4) to the long-range region, which will be discussed in detail later. Each distribution is shifted to have zero associated yield at its minimum to represent the correlated portion of the associated yield. The implementation of the zero-yield-at-minimum (ZYAM) procedure is detailed in Ref. [28]. Selection of a fixed p_T^{trig} and p_T^{assoc} range of both 1–3 GeV is shown for the long-range region (top) and short- minus long-range region (bottom). As illustrated in Fig. 2, the near-side long-range signal remains nearly constant in $\Delta\eta$. Therefore, by taking a difference of 1D $\Delta\phi$ projections between the short-range and long-range region, the near-side jet correlations can be extracted. As shown in the bottom panels of Fig. 3, the magnitude of the near-side jet peak appears to be larger for K^0_S–$h^{\pm}$ than $\Lambda/\overline{\Lambda}$–$h^{\pm}$, both of which are smaller than $h^{\pm}$–$h^{\pm}$ (dominated by $\pi^{\pm}$–$\pi^{\pm}$) correlations. This may be related to the fact that heavier trigger particles carry a larger fraction of jet energy, resulting in less remaining energy to be shared by associated particles. For $N_{trk}^{offline} < 35$, no near-side correlations are observed in the long-range region for any particle species.

Recently, the v_2 anisotropy harmonic for charged pions, kaons, and protons is studied using

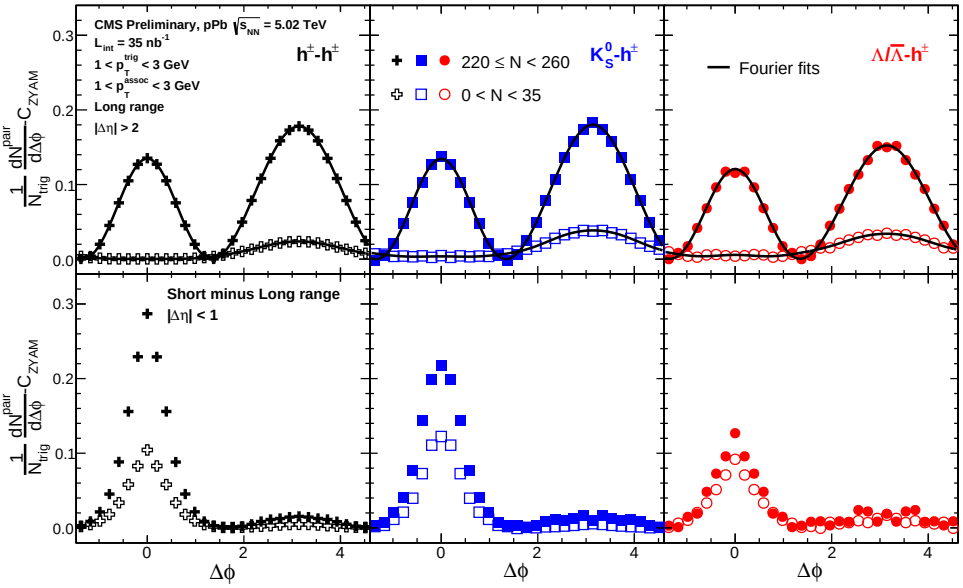

Figure 3: the 1D $\Delta\phi$ correlation functions of the pPb data after applying the ZYAM procedure, in the multiplicity range $N_{\mathrm{trk}}^{\mathrm{offline}} < 35$ (open) and $220 \leq N_{\mathrm{trk}}^{\mathrm{offline}} < 260$ (filled), for $\mathrm{K}^0_{\mathrm{S}}$ (left), $\Lambda/\overline{\Lambda}$ (middle), and unidentified charged particle (right) as a trigger, respectively. Selection of a fixed $p_{\mathrm{T}}^{\mathrm{trig}}$ and $p_{\mathrm{T}}^{\mathrm{assoc}}$ range of both 1–3 GeV is shown for the long-range (top) and short-range (bottom) regions. The lines on the top panels correspond to the Fourier fits including the first three terms.

two-particle correlations in pPb collisions [36], which are found to be qualitatively consistent with hydrodynamic models [37, 38]. In this paper, the elliptic (v_2) and triangular (v_3) flow harmonics of $\mathrm{K}^0_{\mathrm{S}}$ and $\Lambda/\overline{\Lambda}$ are extracted from a Fourier decomposition of 1D $\Delta\phi$ correlation functions for the long-range region ($|\Delta\eta| > 2$) in a significantly larger sample of pPb collisions such that the particle species dependence of v_n can be investigated in detail. In Figure 4, the v_2 signals of $\mathrm{K}^0_{\mathrm{S}}$ and $\Lambda/\overline{\Lambda}$ are extracted as a function of p_{T} for the three lowest multiplicity ranges in 5.02 TeV PbPb and 2.76 TeV pPb collisions. These data are recorded using a minimum bias trigger. For the first two lowest multiplicity ranges, the v_2 values of $\mathrm{K}^0_{\mathrm{S}}$ and $\Lambda/\overline{\Lambda}$ are largely identical within statistical uncertainties. As there is no evident long-range near-side correlation seen in these low-multiplicity events, the extracted v_2 largely reflects back-to-back jet correlations on the away side. However, moving to the higher multiplicity range $60 \leq N_{\mathrm{trk}}^{\mathrm{offline}} < 120$, a deviation of v_2 between $\mathrm{K}^0_{\mathrm{S}}$ and $\Lambda/\overline{\Lambda}$ starts emerging. A higher v_2 value of $\mathrm{K}^0_{\mathrm{S}}$ than $\Lambda/\overline{\Lambda}$ is seen at $p_{\mathrm{T}} \lesssim 2$ GeV. For $p_{\mathrm{T}} \gtrsim 2$ GeV, this order is reversed. This is consistent with the observation by the ALICE collaboration in 0–20% centrality pPb collisions at $\sqrt{s_{NN}}$ = 5.02 TeV [36], where lighter particles show stronger elliptic low at lower p_{T}, and baryons have a larger v_2 than mesons at higher p_{T}. A similar trend is first observed in AA collisions at RHIC [39, 40].

The separation of the v_2 values between $\mathrm{K}^0_{\mathrm{S}}$ and $\Lambda/\overline{\Lambda}$ is even more pronounced for higher multiplicity ranges, as shown in Fig. 5 (top) as a function of p_{T} in 5.02 TeV pPb collisions. The previous published v_2 data of unidentified charged particles are also shown in open cross markers for comparison purposes. In the lower-p_{T} region of $\lesssim 2$ GeV for all high-multiplicity ranges, the v_2 of $\mathrm{K}^0_{\mathrm{S}}$ is bigger than that of $\Lambda/\overline{\Lambda}$ at a given p_{T} value. Both of them are consistently below the v_2 values of unidentified charged particles. As most charged particles are pions, the data indicate that lighter particle species exhibit a stronger azimuthal anisotropy signal. At higher p_{T} above about 2 GeV, the v_2 of $\Lambda/\overline{\Lambda}$ becomes larger than that of $\mathrm{K}^0_{\mathrm{S}}$. The unidentified charged

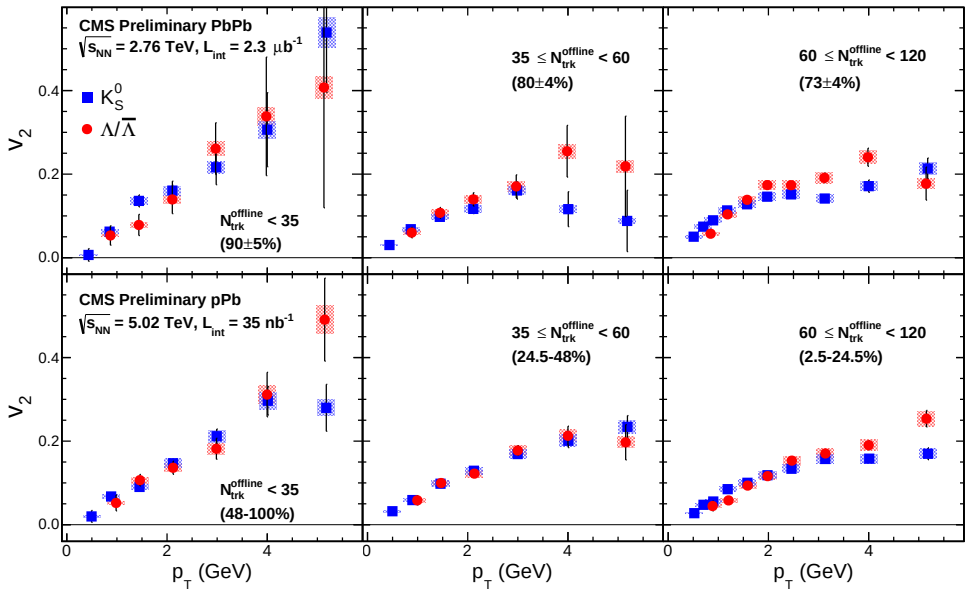

Figure 4: The v_2 results for K^0_S (filled squares) and $\Lambda/\overline{\Lambda}$ (filled circles) as a function of p_T for three multiplicity ranges obtained from minimum bias triggered PbPb sample at $\sqrt{s_{NN}}$ = 2.76 TeV (top row) and pPb sample at $\sqrt{s_{NN}}$ = 5.02 TeV (bottom row). The error bars correspond to statistical uncertainties, while the shaded areas denote the systematic uncertainties.

particle v_2 (dominated by $\pi^{\pm}$) falls between the values of two identified strange hadron species, but much closer to the v_2 of K^0_S mesons.

The scaling behavior of v_2 divided by the number of constituent quarks as a function of transverse kinetic energy per quark, KE_T/n_q, is investigated for high-multiplicity pPb events in the middle row of Fig. 5. After scaling by the number of quarks, the v_2 data of K^0_S and $\Lambda/\overline{\Lambda}$ approximately fall on the same curve. This can be seen directly by taking the ratios of n_q-scaled v_2 to a smooth polynomial fit function through the K^0_S data, as shown in the bottom of Fig. 5. The scaling holds better than 10% over most of the KE_T/n_q range, except for $KE_T/n_q < 0.2$ GeV where the deviation grows to about 20%. In AA collisions, this behavior is conjectured to be related to the quark recombination [41–43], which postulates that collective flow is developed among constituent quarks first before they combine into final-state hadrons.

The study of identified particle v_2 and its scaling behavior is repeated in 2.76 TeV PbPb data over the same multiplicity ranges as for the pPb data, shown in Fig. 6. The average centrality ranges of PbPb data are indicated on the plots, which are mostly in the peripheral range of 60–100% centrality. Qualitatively similar particle-species dependence of v_2 is observed. However, the n_q-scaled v_2 data in PbPb at similar multiplicities suggest a stronger violation of constituent quark number scaling than what is observed in pPb, especially at high KE_T/n_q range. This is also observed in peripheral AuAu collisions at RHIC, while the scaling holds better for central AuAu collisions [40].

The triangular flow harmonic, v_3, of K^0_S and $\Lambda/\overline{\Lambda}$ are also extracted in 5.02 TeV pPb and 2.76 TeV PbPb collisions, shown in Fig. 7. Due to limited statistical precision, only the result in the multiplicity range $185 \leq N^{\text{offline}}_{\text{trk}} < 350$ is presented. A similar species dependence of v_3 to that of v_2 is observed and, within the statistical uncertainties, the scaled v_3 values by the constituent quark number for K^0_S and $\Lambda/\overline{\Lambda}$ match at the level of 20% over the full KE_T/n_q range. Future higher luminosity pPb will be essential to better examine the constituent quark number scaling for higher-order anisotropy harmonics (v_n, $n > 2$).

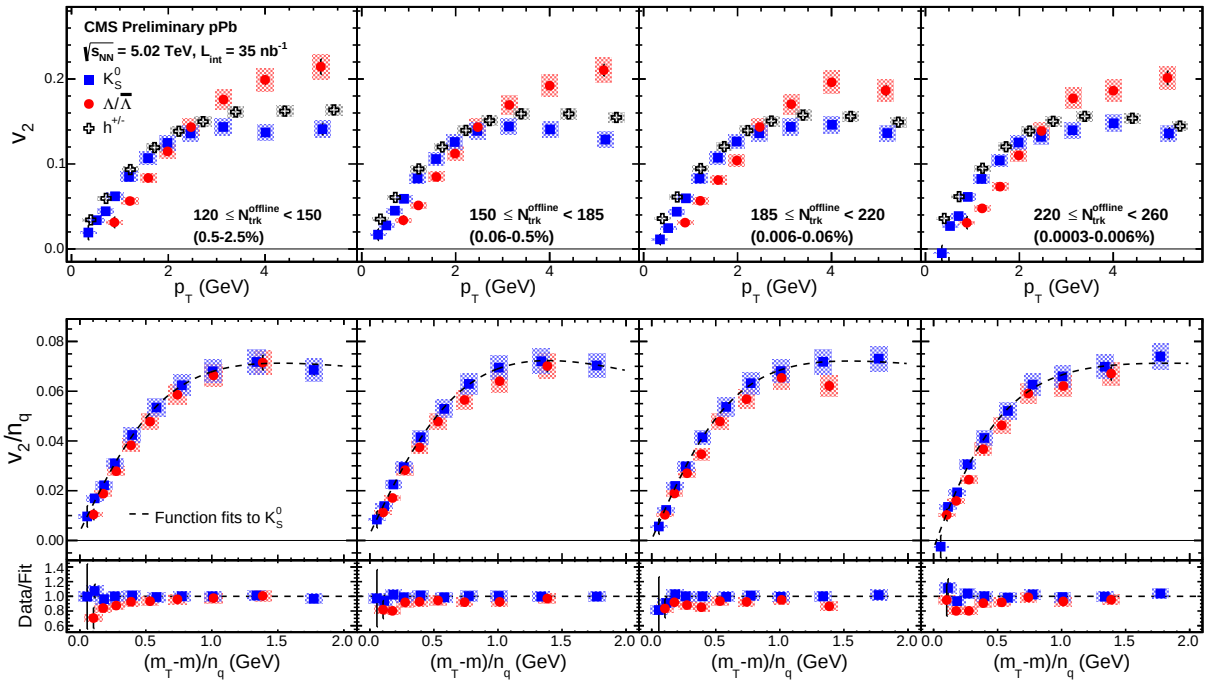

Figure 5: Top row: The v_2 results for K^0_S (filled squares), $\Lambda/\overline{\Lambda}$ (filled circles), and unidentified charged particles (open crosses) as a function of p_T for four multiplicity ranges obtained from high-multiplicity triggered pPb sample at $\sqrt{s_{NN}}$ = 5.02 TeV. Middle row: the v_2/n_q ratios for K^0_S (filled squares) and $\Lambda/\overline{\Lambda}$ (filled circles) as a function of $(m_T - m)/n_q$. Bottom row: ratios of v_2/n_q for K^0_S and $\Lambda/\overline{\Lambda}$ to a smooth fit function of v_2/n_q for K^0_S as a function of $(m_T - m)/n_q$. The error bars correspond to statistical uncertainties, while the shaded areas denote the systematic uncertainties.

7 Summary

In summary, the CMS experiment presented the measurements of two-particle correlations with an identified K^0_S or $\Lambda/\overline{\Lambda}$ trigger particle over a broad pseudorapidity coverage in pPb collisions at $\sqrt{s_{NN}}$ = 5.02 TeV and PbPb collisions at $\sqrt{s_{NN}}$ = 2.76 TeV. With the implementation of a unique high-multiplicity trigger during the LHC 2013 pPb run, the identified particle correlation data in pPb collisions are explored over a broad particle multiplicity range, which is comparable to that covered by 60–100% centrality PbPb collisions. The observed long-range ($|\Delta\eta| > 2$) correlations are quantified in terms of azimuthal anisotropy Fourier harmonics (v_n) motivated by hydrodynamic models. In low-multiplicity pPb and PbPb events, similar v_2 values of K^0_S and $\Lambda/\overline{\Lambda}$ is observed, which are primarily contributed by back-to-back jet correlations. Moving to higher-multiplicity region, a particle species dependence of v_2 and v_3 is observed between K^0_S and $\Lambda/\overline{\Lambda}$. For $p_T \lesssim 2$ GeV, the K^0_S v_n is found to be larger than that of $\Lambda/\overline{\Lambda}$, while this order is reversed for higher-p_T region. This behavior is consistent with what is seen previously in pPb collisions for identified charged hadrons, and also in AA collisions at RHIC and the LHC. Furthermore, the constituent quark number scaling of v_2 and v_3 between K^0_S and $\Lambda/\overline{\Lambda}$ particles is investigated for PbPb and high-multiplicity triggered pPb events. The v_n data, scaled by the number of constituent quarks, as a function of transverse kinetic energy per quark for the two particle species is found to fall on the same curve within 10–15% in pPb collisions. In PbPb, a larger deviation of quark number scaling (up to 20–25%) than that of pPb data is seen, which is similar to the observation in peripheral AuAu collisions at RHIC. The high precision data of identified particle correlations presented for high-multiplicity pPb

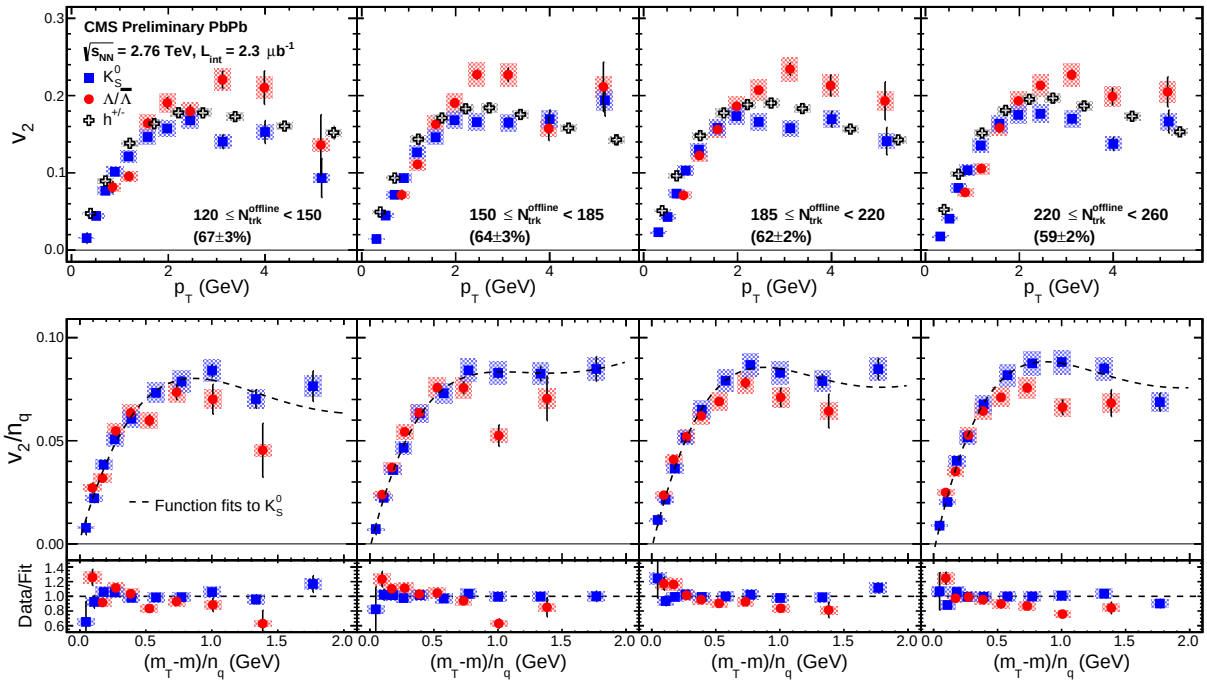

Figure 6: Top row: the v_2 results for K^0_S (filled squares), $\Lambda/\overline{\Lambda}$ (filled circles), and unidentified charged particles (open crosses) as a function of p_T for four multiplicity ranges obtained from minimum bias triggered PbPb sample at $\sqrt{s_{NN}}$ = 2.76 TeV. Middle row: the v_2/n_q ratios for K^0_S (filled squares) and $\Lambda/\overline{\Lambda}$ (filled circles) as a function of $(m_T - m)/n_q$. Bottom row: ratios of v_2/n_q for K^0_S and $\Lambda/\overline{\Lambda}$ to a smooth fit function of v_2/n_q for K^0_S as a function of $(m_T - m)/n_q$. The error bars correspond to statistical uncertainties, while the shaded areas denote the systematic uncertainties.

data over a wide kinematic and acceptance coverage in this paper provide important insight to further explore the possible collective flow origin of long-range correlations, and shed light on models of quark recombination in a deconfined medium of quarks and gluons.

Acknowledgments

We congratulate our colleagues in the CERN accelerator departments for the excellent performance of the LHC and thank the technical and administrative staffs at CERN and at other CMS institutes for their contributions to the success of the CMS effort. In addition, we gratefully acknowledge the computing centres and personnel of the Worldwide LHC Computing Grid for delivering so effectively the computing infrastructure essential to our analyses. Finally, we acknowledge the enduring support for the construction and operation of the LHC and the CMS detector provided by the following funding agencies: BMWF and FWF (Austria); FNRS and FWO (Belgium); CNPq, CAPES, FAPERJ, and FAPESP (Brazil); MES (Bulgaria); CERN; CAS, MoST, and NSFC (China); COLCIENCIAS (Colombia); MSES and CSF (Croatia); RPF (Cyprus); MoER, SF0690030s09 and ERDF (Estonia); Academy of Finland, MEC, and HIP (Finland); CEA and CNRS/IN2P3 (France); BMBF, DFG, and HGF (Germany); GSRT (Greece); OTKA and NIH (Hungary); DAE and DST (India); IPM (Iran); SFI (Ireland); INFN (Italy); NRF and WCU (Republic of Korea); LAS (Lithuania); MOE and UM (Malaysia); CINVESTAV, CONACYT, SEP, and UASLP-FAI (Mexico); MBIE (New Zealand); PAEC (Pakistan); MSHE and NSC (Poland); FCT (Portugal); JINR (Dubna); MON, RosAtom, RAS and RFBR (Russia); MESTD (Serbia); SEIDI and CPAN (Spain); Swiss Funding Agencies (Switzerland); NSC (Taipei); ThEPCenter,

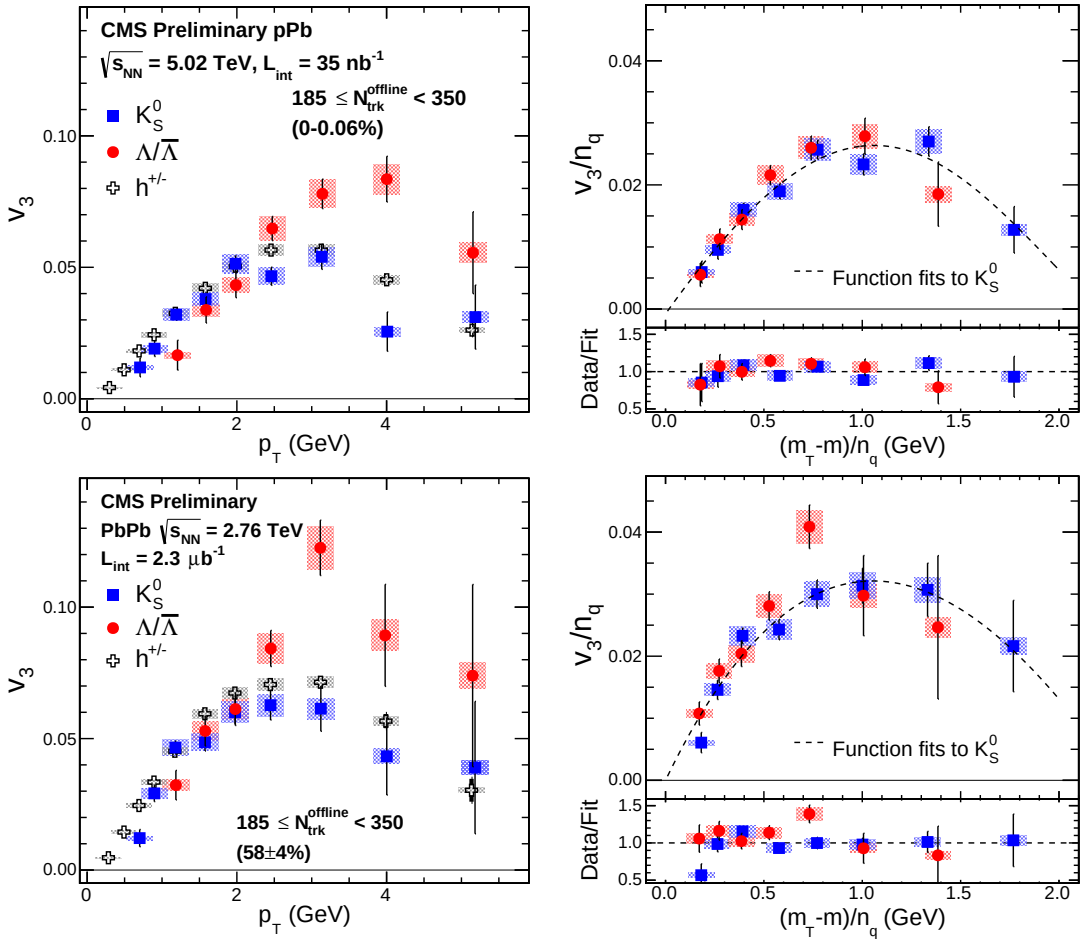

Figure 7: Left: the v_3 results for K^0_S (filled squares), $\Lambda/\overline{\Lambda}$ (filled circles), and unidentified charged particles (open crosses) as a function of p_T for $185 \leq N^{\text{offline}}_{\text{trk}} < 350$ obtained in pPb at $\sqrt{s_{NN}}$ = 5.02 TeV (top) and PbPb as $\sqrt{s_{NN}}$ = 2.76 TeV (bottom). Right: the n_q-scaled v_3 (bottom) values of K^0_S (filled squares) and $\Lambda/\overline{\Lambda}$ (filled circles) as a function of $(m_T - m)/n_q$. Ratios of v_n/n_q to a smooth fit function of v_n/n_q for K^0_S as a function of $(m_T - m)/n_q$ are also shown. The error bars correspond to statistical uncertainties, while the shaded areas denote the systematic uncertainties.

IPST, STAR and NSTDA (Thailand); TUBITAK and TAEK (Turkey); NASU and SFFR (Ukraine); STFC (United Kingdom); DOE and NSF (USA).

Individuals have received support from the Marie-Curie programme and the European Research Council and EPLANET (European Union); the Leventis Foundation; the A. P. Sloan Foundation; the Alexander von Humboldt Foundation; the Belgian Federal Science Policy Office; the Fonds pour la Formation à la Recherche dans l'Industrie et dans l'Agriculture (FRIA-Belgium); the Agentschap voor Innovatie door Wetenschap en Technologie (IWT-Belgium); the Ministry of Education, Youth and Sports (MEYS) of Czech Republic; the Council of Science and Industrial Research, India; the Compagnia di San Paolo (Torino); the HOMING PLUS programme of Foundation for Polish Science, cofinanced by EU, Regional Development Fund; and the Thalis and Aristeia programmes cofinanced by EU-ESF and the Greek NSRF.

References

[1] STAR Collaboration, "Distributions of charged hadrons associated with high transverse momentum particles in pp and Au + Au collisions at $\sqrt{s_{NN}}$ = 200 GeV", *Phys. Rev. Lett.* **95** (2005) 152301, doi:10.1103/PhysRevLett.95.152301, arXiv:nucl-ex/0501016.

[2] STAR Collaboration, "Long range rapidity correlations and jet production in high energy nuclear collisions", *Phys. Rev. C* **80** (2009) 064912, doi:10.1103/PhysRevC.80.064912, arXiv:0909.0191.

[3] PHOBOS Collaboration, "System size dependence of cluster properties from two-particle angular correlations in Cu+Cu and Au+Au collisions at $\sqrt{s_{NN}}$ = 200 GeV", *Phys. Rev. C* **81** (2010) 024904, doi:10.1103/PhysRevC.81.024904, arXiv:0812.1172.

[4] PHOBOS Collaboration, "High transverse momentum triggered correlations over a large pseudorapidity acceptance in Au+Au collisions at $\sqrt{s_{NN}}$ = 200 GeV", *Phys. Rev. Lett.* **104** (2010) 062301, doi:10.1103/PhysRevLett.104.062301, arXiv:0903.2811.

[5] STAR Collaboration, "Three-particle coincidence of the long range pseudorapidity correlation in high energy nucleus-nucleus collisions", *Phys. Rev. Lett.* **105** (2010) 022301, doi:10.1103/PhysRevLett.105.022301, arXiv:0912.3977.

[6] CMS Collaboration, "Long-range and short-range dihadron angular correlations in central PbPb collisions at a nucleon-nucleon center of mass energy of 2.76 TeV", *JHEP* **07** (2011) 076, doi:10.1007/JHEP07(2011)076, arXiv:1105.2438.

[7] CMS Collaboration, "Centrality dependence of dihadron correlations and azimuthal anisotropy harmonics in PbPb collisions at $\sqrt{s_{NN}}$ = 2.76 TeV", *Eur. Phys. J. C* **72** (2012) 2012, doi:10.1140/epjc/s10052-012-2012-3, arXiv:1201.3158.

[8] ALICE Collaboration, "Harmonic decomposition of two-particle angular correlations in Pb-Pb collisions at $\sqrt{s_{NN}}$ = 2.76 TeV", *Phys. Lett. B* **708** (2012) 249, doi:10.1016/j.physletb.2012.01.060, arXiv:1109.2501.

[9] ATLAS Collaboration, "Measurement of the azimuthal anisotropy for charged particle production in $\sqrt{s_{NN}}$ = 2.76 TeV lead-lead collisions with the ATLAS detector", *Phys. Rev. C* **86** (2012) 014907, doi:10.1103/PhysRevC.86.014907, arXiv:1203.3087.

[10] CMS Collaboration, "Studies of azimuthal dihadron correlations in ultra-central PbPb collisions at $\sqrt{s_{NN}}$ = 2.76 TeV", *JHEP* **02** (2014) 088, doi:10.1007/JHEP02(2014)088, arXiv:1312.1845.

[11] J.-Y. Ollitrault, "Anisotropy as a signature of transverse collective flow", *Phys. Rev. D* **46** (1992) 229, doi:10.1103/PhysRevD.46.229.

[12] S. Voloshin and Y. Zhang, "Flow study in relativistic nuclear collisions by Fourier expansion of azimuthal particle distributions", *Z. Phys. C* **70** (1996) 665, doi:10.1007/s002880050141, arXiv:hep-ph/9407282.

[13] B. Alver and G. Roland, "Collision geometry fluctuations and triangular flow in heavy-ion collisions", *Phys. Rev. C* **81** (2010) 054905, doi:10.1103/PhysRevC.82.039903,10.1103/PhysRevC.81.054905, arXiv:1003.0194.

[14] B. H. Alver, C. Gombeaud, M. Luzum, and J.-Y. Ollitrault, "Triangular flow in hydrodynamics and transport theory", *Phys. Rev. C* **82** (2010) 034913, doi:10.1103/PhysRevC.82.034913, arXiv:1007.5469.

[15] B. Schenke, S. Jeon, and C. Gale, "Elliptic and triangular flow in event-by-event D=3+1 viscous hydrodynamics", *Phys. Rev. Lett.* **106** (2011) 042301, doi:10.1103/PhysRevLett.106.042301, arXiv:1009.3244.

[16] Z. Qiu, C. Shen, and U. Heinz, "Hydrodynamic elliptic and triangular flow in Pb-Pb collisions at $\sqrt{s_{NN}}$ = 2.76 TeV", *Phys. Lett. B* **707** (2012) 151, doi:10.1016/j.physletb.2011.12.041, arXiv:1110.3033.

[17] CMS Collaboration, "Observation of Long-Range Near-Side Angular Correlations in Proton-Proton Collisions at the LHC", *JHEP* **09** (2010) 091, doi:10.1007/JHEP09(2010)091, arXiv:1009.4122.

[18] CMS Collaboration, "Observation of long-range near-side angular correlations in proton-lead collisions at the LHC", *Phys. Lett. B* **718** (2013) 795, doi:10.1016/j.physletb.2012.11.025, arXiv:1210.5482.

[19] ALICE Collaboration, "Long-range angular correlations on the near and away side in pPb collisions at $\sqrt{s_{NN}}$ = 5.02 TeV", *Phys. Lett. B* **719** (2013) 29, doi:10.1016/j.physletb.2013.01.012, arXiv:1212.2001.

[20] ATLAS Collaboration, "Observation of Associated Near-side and Away-side Long-range Correlations in $\sqrt{s_{NN}}$ = 5.02 TeV Proton-lead Collisions with the ATLAS Detector", *Phys. Rev. Lett.* **110** (2013) 182302, doi:10.1103/PhysRevLett.110.182302, arXiv:1212.5198.

[21] PHENIX Collaboration, "Quadrupole Anisotropy in Dihadron Azimuthal Correlations in Central d+Au Collisions at $\sqrt{s_{NN}}$200 GeV", *Phys. Rev. Lett.* **111** (2013) 212301, doi:10.1103/PhysRevLett.111.212301, arXiv:1303.1794.

[22] W. Li, "Observation of a 'Ridge' correlation structure in high multiplicity proton-proton collisions: A brief review", *Mod. Phys. Lett. A* **27** (2012) 1230018, doi:10.1142/S0217732312300182, arXiv:1206.0148.

[23] P. Bozek, "Collective flow in p-Pb and d-Pd collisions at TeV energies", *Phys. Rev. C* **85** (2012) 014911, doi:10.1103/PhysRevC.85.014911, arXiv:1112.0915.

[24] P. Bozek and W. Broniowski, "Correlations from hydrodynamic flow in pPb collisions", *Phys. Lett. B* **718** (2013) 1557, doi:10.1016/j.physletb.2012.12.051, arXiv:1211.0845.

[25] K. Dusling and R. Venugopalan, "Explanation of systematics of CMS p+Pb high multiplicity di-hadron data at $\sqrt{s_{NN}}$ = 5.02 TeV", *Phys. Rev. D* **87** (2013) 054014, doi:10.1103/PhysRevD.87.054014, arXiv:1211.3701.

[26] K. Dusling and R. Venugopalan, "Evidence for BFKL and saturation dynamics from dihadron spectra at the LHC", *Phys. Rev. D* **87** (2013) 051502, doi:10.1103/PhysRevD.87.051502, arXiv:1210.3890.

[27] ATLAS Collaboration, "Measurement with the ATLAS detector of multi-particle azimuthal correlations in p+Pb collisions at $\sqrt{s_{NN}}$5.02 TeV", *Phys. Lett. B* **725** (2013) 60, doi:10.1016/j.physletb.2013.06.057, arXiv:1303.2084.

[28] CMS Collaboration, "Multiplicity and transverse momentum dependence of two- and four-particle correlations in pPb and PbPb collisions", *Phys. Lett. B* **724** (2013) 213, doi:10.1016/j.physletb.2013.06.028, arXiv:1305.0609.

[29] STAR Collaboration, "Experimental and theoretical challenges in the search for the quark gluon plasma: The STAR Collaboration's critical assessment of the evidence from RHIC collisions", *Nucl. Phys. A* **757** (2005) 102, doi:10.1016/j.nuclphysa.2005.03.085, arXiv:nucl-ex/0501009.

[30] PHENIX Collaboration, "Formation of dense partonic matter in relativistic nucleus-nucleus collisions at RHIC: Experimental evaluation by the PHENIX collaboration", *Nucl. Phys. A* **757** (2005) 184, doi:10.1016/j.nuclphysa.2005.03.086, arXiv:nucl-ex/0410003.

[31] PHENIX Collaboration, "Elliptic flow of identified hadrons in Au+Au collisions at $\sqrt{s_{NN}}$ = 200-GeV", *Phys. Rev. Lett.* **91** (2003) 182301, doi:10.1103/PhysRevLett.91.182301, arXiv:nucl-ex/0305013.

[32] STAR Collaboration, "Azimuthal anisotropy in Au+Au collisions at $\sqrt{s_{NN}}$ = 200-GeV", *Phys. Rev. C* **72** (2005) 014904, doi:10.1103/PhysRevC.72.014904, arXiv:nucl-ex/0409033.

[33] P. Huovinen et al., "Radial and elliptic flow at RHIC: Further predictions", *Phys. Lett. B* **503** (2001) 58, doi:10.1016/S0370-2693(01)00219-2, arXiv:hep-ph/0101136.

[34] P. F. Kolb and U. W. Heinz, "Hydrodynamic description of ultrarelativistic heavy ion collisions", arXiv:nucl-th/0305084.

[35] C. Shen, U. Heinz, P. Huovinen, and H. Song, "Radial and elliptic flow in Pb+Pb collisions at the Large Hadron Collider from viscous hydrodynamic", *Phys. Rev. C* **84** (2011) 044903, doi:10.1103/PhysRevC.84.044903, arXiv:1105.3226.

[36] ALICE Collaboration, "Long-range angular correlations of pi, K and p in p–Pb collisions at $\sqrt{s_{NN}}$ = 5.02 TeV", *Phys. Lett. B* **726** (2013) 164, doi:10.1016/j.physletb.2013.08.024, arXiv:1307.3237.

[37] K. Werner et al., "Evidence for flow in pPb collisions at 5 TeV from v_2 mass splitting", arXiv:1307.4379.

[38] P. Bozek, W. Broniowski, and G. Torrieri, "Mass hierarchy in identified particle distributions in proton-lead collisions", *Phys. Rev. Lett.* **111** (2013) 172303, doi:10.1103/PhysRevLett.111.172303, arXiv:1307.5060.

[39] STAR Collaboration, "Mass, quark-number, and $\sqrt{s_{NN}}$ dependence of the second and fourth flow harmonics in ultra-relativistic nucleus-nucleus collisions", *Phys. Rev. C* **75** (2007) 054906, doi:10.1103/PhysRevC.75.054906, arXiv:nucl-ex/0701010.

[40] PHENIX Collaboration, "Deviation from quark-number scaling of the anisotropy parameter v_2 of pions, kaons, and protons in Au+Au collisions at $\sqrt{s_{NN}}$ = 200 GeV", *Phys. Rev. C* **85** (2012) 064914, doi:10.1103/PhysRevC.85.064914, arXiv:1203.2644.

[41] D. Molnar and S. A. Voloshin, "Elliptic flow at large transverse momenta from quark coalescence", *Phys. Rev. Lett.* **91** (2003) 092301, doi:10.1103/PhysRevLett.91.092301, arXiv:nucl-th/0302014.

[42] V. Greco, C. Ko, and P. Levai, "Parton coalescence and anti-proton / pion anomaly at RHIC", *Phys. Rev. Lett.* **90** (2003) 202302, doi:10.1103/PhysRevLett.90.202302, arXiv:nucl-th/0301093.

[43] R. Fries, B. Muller, C. Nonaka, and S. Bass, "Hadronization in heavy ion collisions: Recombination and fragmentation of partons", *Phys. Rev. Lett.* **90** (2003) 202303, doi:10.1103/PhysRevLett.90.202303, arXiv:nucl-th/0301087.

[44] CMS Collaboration, "The CMS experiment at the CERN LHC", *JINST* **03** (2008) S08004, doi:10.1088/1748-0221/3/08/S08004.

[45] Geant4 Collaboration, "Geant4: A simulation toolkit", *Nucl. Instrum. and Meth. A* **506** (2003) 250, doi:10.1016/S0168-9002(03)01368-8.

[46] CMS Collaboration, "Measurement of the inelastic proton-lead cross section at $\sqrt{s_{NN}}$ = 5.02 TeV", CMS Physics Analysis Summary CMS-PAS-FSQ-13-006, 2013.

[47] S. Porteboeuf, T. Pierog, and K. Werner, "Producing Hard Processes Regarding the Complete Event: The EPOS Event Generator", (2010). arXiv:1006.2967.

[48] M. Gyulassy and X.-N. Wang, "HIJING 1.0: A Monte Carlo program for parton and particle production in high-energy hadronic and nuclear collisions", *Comput. Phys. Commun.* **83** (1994) 307, doi:10.1016/0010-4655(94)90057-4, arXiv:nucl-th/9502021.

[49] CMS Collaboration, "Tracking and Vertexing Results from First Collisions", CMS Physics Analysis Summary CMS-PAS-TRK-10-001, 2010.

[50] CMS Collaboration, "Azimuthal anisotropy of charged particles at high transverse momenta in PbPb collisions at $\sqrt{s_{NN}}$ = 2.76 TeV", *Phys. Rev. Lett.* **109** (2012) 022301, doi:10.1103/PhysRevLett.109.022301, arXiv:1204.1850.

[51] CMS Collaboration, "Strange Particle Production in pp Collisions at $\sqrt{s}$ = 0.9 and 7 TeV", *JHEP* **05** (2011) 064, doi:10.1007/JHEP05(2011)064, arXiv:1102.4282.